Dynamical study of adsorbate-induced restructuring kinetics in bimetallic catalysts using the PdAu(111) model system

Chen Zhou,[†,‡] Hio Tong Ngan,[¶] Jin Soo Lim,[*,§] Zubin Darbari,[†,‡] Adrian Lewandowski,[§] Dario J. Stacchiola,[†] Boris Kozinsky,[‖,⊥] Philippe Sautet,[*,¶,#] and Jorge Anibal Boscoboinik[*,†]

[†] Center for Functional Nanomaterials, Brookhaven National Laboratory, Upton, New York 11973, United States of America

[‡] Department of Materials Science and Chemical Engineering, Stony Brook University, Stony Brook, New York 11790, United States of America

[¶] Department of Chemical and Biomolecular Engineering, University of California, Los Angeles, Los Angeles, California 90095, United States of America

[§] Department of Chemistry and Chemical Biology, Harvard University, Cambridge, Massachusetts 02138, United States of America

[‖] Harvard John A. Paulson School of Engineering and Applied Sciences, Harvard University, Cambridge, Massachusetts 02138, United States of America

[⊥] Robert Bosch LLC, Research and Technology Center, Cambridge, Massachusetts 02139, United States of America

[#] Department of Chemistry and Biochemistry, University of California, Los Angeles, Los Angeles, California 90095, United States of America

* Corresponding authors

Email: jboscoboinik@bnl.gov, sautet@ucla.edu, limjs@g.harvard.edu

Graphical abstract

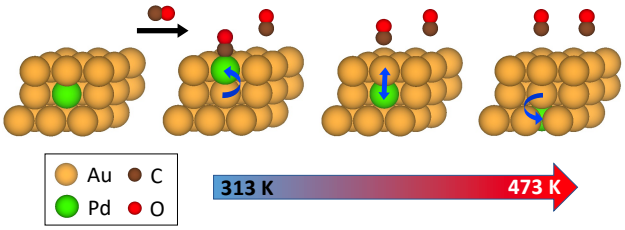

Abstract

The dynamic restructuring of bimetallic catalysts plays a crucial role in their catalytic activity and selectivity. In particular, catalyst pretreatment with species such as carbon monoxide and oxygen has been shown to be an effective strategy for tuning the surface composition and morphology. Mechanistic and kinetic understanding of such restructuring are fundamental to the chemistry and engineering of surface active sites but have remained challenging due to the large structural, chemical, and temporal degrees of freedom. Here, we combine time-resolved temperature-programmed infrared reflection absorption spectroscopy, *ab initio* thermodynamics, and machine-learning molecular dynamics to uncover previously unidentified timescale and kinetic parameters of *in situ* restructuring in Pd/Au(111), a highly relevant model system for dilute Pd-in-Au nanoparticle catalysts. The key innovation lies in utilizing CO not only as a chemically sensitive probe of surface Pd, but also as an agent that induces restructuring of the surface. Upon annealing in vacuum, as-deposited Pd islands became encapsulated by Au and partially dissolved into the subsurface, leaving behind isolated Pd monomers on the surface. Subsequent exposure to 0.1 mbar CO enabled Pd monomers to repopulate the surface up to 373 K, above which complete Pd dissolution occurred by 473 K, with apparent activation energies of 0.14 and 0.48 eV, respectively. These restructuring processes occurred over the span of ~1000 s at a given temperature. Such a minute-timescale dynamics not only elucidates the fluxional nature of alloy catalysts but also presents an opportunity to fine-tune the surface at moderate temperature and pressure conditions.

1. Introduction

Bimetallic catalysts are employed in many chemical transformations, including selective hydrogenation,[1,2] reforming,[3,4] coupling,[5] and oxidation reactions,[6] because of their enhanced catalytic performance compared to their monometallic counterparts.[7] In particular, PdAu alloy catalysts have garnered much attention and research due to their effectiveness in catalyzing a variety of reactions, such as CO oxidation,[6] hydrogen peroxide synthesis,[8,9] cyclomerization of acetylene to benzene,[10] and ethanol electrooxidation.[11,12] In dilute alloys, catalytic activity and selectivity are governed by the geometry of the active sites, i.e. atomic ensembles of the active metal. Combined experimental characterizations and first-principles modeling have played a key role in establishing optimal ensembles for a given reaction.[13,14] In Au hosts, for example, hydrogen turnover remains optimal in the presence of Pd monomers and dimers,[15] whereas the selectivity behavior of e.g. ethanol dehydrogenation shifts as a function of the Pd ensemble distribution.[16] As such, a fundamental understanding of alloy surface structures at the atomic level lies central to rational catalyst design efforts across theory and experiment.[16–18]

Alloy surfaces are inherently dynamic at reaction temperatures of interest. Compared to the originally synthesized state, the surface composition and morphology can change dramatically upon annealing,[19] pretreatments,[20] or during the reaction itself.[21–24] In the case of dilute Pd in Au, it is catalytically desirable to maintain active Pd on the surface of relatively inert Au. However, because Pd has a higher surface free energy than Au (Pd = 2.05 J/m^2; Au = 1.63 J/m^2),[25] Pd thermodynamically prefers to dissolve into Au under reducing conditions. Using scanning tunneling microscopy (STM), a previous study of 1 at.% Pd deposited on Au(111) demonstrated that the distribution of Pd ensembles can be tuned by careful control of the deposition temperature.[17] Specifically, a mixture of Pd islands and smaller Pd ensembles were obtained upon deposition at ~300 K, and Pd dissolved into the bulk of Au upon annealing at 450 K.

Segregation of Pd back to the surface has been observed at moderate temperatures in the presence of strongly bound adsorbates such as CO and O.[20] Here, preferential adsorption of these species on Pd sites allows Pd to be stabilized on the surface and lowers the overall surface free energy.[21] In particular, CO-induced reverse segregation has also been reported in related bimetallic systems, such as Pd/Au(111),[26] Au/Pd(100),[27] and AuPt nanoparticles.[28] Using diffuse reflectance infrared Fourier transform spectroscopy (DRIFTS) and first-principles based Monte Carlo simulations, a recent study of single-atom alloy $PdAu/SiO_2$ demonstrated that CO partial pressure and temperature can be used to control the catalyst selectivity by reversibly tuning the Pd ensemble distribution.[16] Such restructuring phenomena can be understood in terms of four competing thermodynamic factors within the quasi-chemical approximation: elemental differences of the constituent metals (surface energy, strain energy, alloying energy)[29] and the adsorption energy of chemical species.[30]

However, mechanistic and kinetic studies of surface restructuring remain scarce and challenging due to the large underlying configurational space and timescale that need to be explored.[19,31–37] In this regard, single-crystal model systems offer a promising platform for accurate and controlled investigation of bimetallic surfaces, especially for dilute alloys where host metal atoms can be substituted systematically by dopant atoms.[31,33,37–43] Moreover, CO acts as an

effective probe molecule to detect the presence of surface ensembles due to its preferential binding to the active metal (such as Pd) over the more inert host metal (such as Au),[19,20] provided that the temperature is low enough to limit thermal mobility and prevent any restructuring induced by CO itself.[44–46] CO adsorption on Pd sites has been studied extensively,[47] and the binding sites can be differentiated through CO vibrational frequencies from infrared spectroscopy.

In this work, we uncover the kinetic parameters and the timescale of CO-induced restructuring in dilute Pd-in-Au catalysts using single-crystal model systems. Extraction of both structural and dynamical information was enabled by combining time-resolved temperature-programmed infrared reflection absorption spectroscopy (IRRAS), *ab initio* thermodynamics, and machine-learning molecular dynamics (MD) simulations. Varying amounts of Pd were deposited on Au(111) and annealed, using CO adsorption at low temperature to probe the surface. Then, elevated pressure of CO was introduced and the temperature was increased in steps, each time monitoring the CO signal to track the surface Pd content. As such, CO was utilized both as a chemically sensitive surface probe and as an agent to induce the restructuring of the surface.

Our surface science investigation reveals the highly dynamic nature of the PdAu surface as a function of the Pd coverage, CO pressure, temperature, and time. At low Pd coverage, the surface mostly consisted of isolated Pd atoms after short annealing at 473 K. MD simulations revealed the atomic mechanisms by which Pd islands became encapsulated by Au and dissolved into the subsurface, leaving behind surface Pd monomers. From temperature-programmed IRRAS, exposure to 0.1 mbar of CO resulted in an increased surface concentration of Pd monomers up to 373 K. Above this temperature, the fraction of Pd monomers with adsorbed CO decreases and Pd starts dissolving into the sublayers, completing the process by 473 K. The CO-induced segregation and the dissolution after CO desorption exhibited apparent activation energies of 0.14 and 0.48 eV, respectively. These restructuring processes occurred over the span of ~1000 s at a given temperature. Such minute-timescale dynamics at moderate temperature and pressure conditions highlight a potential avenue to fine-tune the compositions of catalytic surfaces.

Our approach combining time-resolved experiments, simulations, and theoretical modeling can be applied to study the dynamical behavior of complex bimetallic catalysts under reaction conditions of interest. While this work focuses on the effect of CO on Pd-in-Au alloys, our results provide the foundation for a general approach to understanding the precise mechanisms by which adsorbate species present during chemical reactions induce restructuring of multi-metallic systems, which is of relevance to a multitude of catalytic processes, including coupling, oxidation, dehalogenation, reforming, etc.

2. Experimental section

2.1. Material preparation

PdAu alloys with various Pd coverages (in ML = monolayer) were prepared using single-crystal Au(111) as a substrate. The Au single crystal was first cleaned by cycles of Ar^+ sputtering (2×10^{-5} mbar; 1.1 keV) with sequential annealing in ultrahigh vacuum (UHV) (5 min at 923 K, followed by 20 min at 673 K) until no contamination was found with X-ray photoelectron spectroscopy (XPS) measurements. Then, Pd was deposited onto the cleaned Au(111) from a Pd rod using an e-beam heating evaporator (SPECS EBE-4) at a constant flux of 10 nA at room temperature. The deposition was conducted in a preparation chamber (base pressure 1×10^{-9} mbar) connected to XPS and IRRAS chambers within the same instrument. Prior to each IR measurement, we conducted 10-min evaporation followed by XPS measurements to calibrate the rate of Pd deposition. The measured areas under XPS (Pd $3p_{3/2}$ and Au $4f_{7/2}$ for Pd and Au, respectively) were corrected specifically to Pd (dopant) on Au (host), with the assumption that all Pd atoms remain on the surface right after deposition. More details can be found in a previous work where Pd coverage on Ag was calibrated by a similar method.[20]

2.2. X-ray photoelectron spectroscopy (XPS)

XPS experiments were performed using a system equipped with a SPECS PHOIBOS NAP 150 hemispherical analyzer, described elsewhere.[48] For Pd coverage calibration, the peak areas of Pd 3*p* and Au 4*f* states were obtained by applying a Shirley background to the region of interest.

2.3. Infrared reflection absorption spectroscopy (IRRAS)

IRRAS experiments were carried out in a chamber with a base pressure of $< 1\times10^{-8}$ mbar. Gas doses are reported in Langmuir, defined as 1 L = 1×10^{-6} Torr·s. The sample temperature was measured using a thermocouple (type K) attached next to the sample, spot-welded on the sample plate. The sample can be heated up to 800 K using a lamp heater located below the sample plate or cooled down to ~100 K with constant liquid nitrogen flowing through the sample stage. Peak areas were integrated using Origin software by applying a straight line as background.

To understand the Pd ensembles present in our model system and investigate the effect of annealing on surface evolution, the sample was heated to various temperatures starting at 373 K with steps of 50 K, and held for only a few seconds at each annealing step. To minimize the CO-induced reconstruction, the sample was rapidly cooled down to 165 K after each annealing step and IR spectra were measured after a dosage of 100 L CO at this temperature (165 K).

Temperature-programmed IRRAS was conducted after the sample was annealed at 473 K for 10 min in vacuum and cooled down to 313 K. After introducing a constant pressure of CO, the surface was heated in steps of 10 K until the CO signal was lost. At each temperature, multiple

spectra were measured in intervals of 220 s to extract the kinetic parameters of surface restructuring in the presence of CO, assuming a first-order reaction in which the rate depends on the concentration of surface Pd atoms.

To prevent contamination from volatile metal carbonyl species,[49] a heated carbonyl trap was placed before the valve that was used to leak CO into the chamber. No Ni was observed (the most common contaminant), as confirmed by the lack of peak typically located at 2050 cm^{-1} corresponding to CO stretching vibration.

2.4. Density functional theory (DFT)

DFT calculations[50] were performed using plane-wave basis sets[51] as implemented in the Vienna *Ab Initio* Simulation Package (VASP).[52] All structures were optimized via ionic relaxation, with the total energy and forces converged to 10^{-6} eV and 0.02 eV/Å, respectively. A four-layer slab model of a 3×3 unit cell of Au(111) was used. The bottom two layers were fixed at bulk positions to mimic bulk properties. The Brilllouin zone was sampled using a 7×7×1 Monkhorst-Pack *k*-point grid.[53] The Perdew-Burke-Ernzerhof (PBE) parametrization[54] of the generalized gradient approximation (GGA) of the exchange-correlation functional was employed, along with the dDsC dispersion correction[55–57] to account for van der Waals interaction.

PBE functional is known to overestimate the adsorption strength of CO as it misjudges the HOMO-LUMO gap of the molecule.[58] To overcome this limitation, the correction scheme of Mason *et al.*[59] was employed by constructing a scaling relation between CO adsorption energies and the single-triplet excitation energies of gas-phase CO, using five different pseudopotentials. Different cutoff energies for plane-wave basis sets were used depending on the softness of the pseudopotentials (~1.2 times the ENMAX specified in the pseudopotentials). The corrected adsorption energies were obtained by extrapolating to the accurate configuration-interaction value of the excitation energies (6.095 eV).[60]

The calculations of Gibbs free energies include thermal effects, zero-point energies, and entropic contributions (translational, rotational, and vibrational degrees of freedom were taken into account for gaseous CO; only vibrational contributions were considered for the surface species). The Gibbs free energy of adsorption is defined as the change in free energy from an isolated slab and n gaseous CO molecules to a combined system of n CO molecules adsorbed on the slab:

$$G_{\mathrm{ads}} = G\left[n\mathrm{CO}_{(\mathrm{ads})}/\mathrm{PdAu}(111)\right] - G[\mathrm{PdAu}(111)] - nG\left[\mathrm{CO}_{(\mathrm{g})}\right].$$

CO adsorption isotherm was obtained using the Langmuir adsorption equation:

$$\theta_{\mathrm{CO}} = \frac{K_{\mathrm{eq}}P_{\mathrm{CO}}}{1 + K_{\mathrm{eq}}P_{\mathrm{CO}}},$$

where K_{eq} is the equilibrium constant for CO adsorption and P_{CO} is the CO pressure. K_{eq} was calculated as:

$$K_{\mathrm{eq}} = e^{\frac{-\Delta G^{\mathrm{o}}_{\mathrm{ads}}}{k_{\mathrm{B}}T}},$$

where $\Delta G^{\mathrm{o}}_{\mathrm{ads}}$ is the free energy of adsorption under standard conditions, k_{B} is the Boltzmann's constant, and T is the temperature.

2.5. Machine-learning molecular dynamics (MD)

A Gaussian process (GP) model of the Pd/Au potential energy surface was trained on atomic forces from DFT.[19] To generate the training data, we performed *ab initio* molecular dynamics (AIMD) simulation using the PBE functional and the same set-up as described above. The total energy was converged to 10^{-5} eV at each timestep. PBE provides Au lattice constant of 4.16 Å, within <0.1 Å of the experimental benchmark of 4.08 Å.[61] A three-layer slab model of a 7×7 unit cell of Au(111) was employed with a hexagonal Pd_{19} cluster deposited on the top. The Brillouin zone was sampled using a Γ-centered 3×3×1 *k*-point grid. A velocity-Verlet integrator with a time step of δt = 5.0 fs was used to evolve the equations of motion for 15 ps within the canonical (NVT) ensemble. To ensure that diverse atomic environments are encountered, all atoms were mobile with the temperature set at 1100 K (bulk Au melting point = 1337 K)[62] via Nosé-Hoover thermostat (40 δt = 0.2 ps coupling).[63,64]

The training data were selected using an active learning protocol as implemented in the "GP from AIMD" (GPFA) module of the Fast Learning of Atomistic Rare Events (FLARE) library.[65] The two- and three-body multielement kernel is used as the covariance function, with 7.0 and 4.5 Å cutoff for the two- three-body interactions, respectively. The AIMD frames were presented sequentially to the GP, each time predicting all atomic force components. If the predictive standard deviation of any force component exceeded the current noise parameter, the highest uncertainty atomic environment and its force components were added to the training set and the hyperparameters were reoptimized. The final hyperparameters and force field accuracy are described in **Sec. 4**, **SI**.

To produce a fast tabulated force field, the two- and three-body mean predictions were mapped onto cubic spline models.[66] The two-body mean function, a one-dimensional function of the interatomic distance, was mapped with 64 control points. The three-body mean function, a three-dimensional function of the interatomic distances of triplets of atoms, was mapped with a uniform 10×10×10 grid of control points. The resulting potential was implemented as the MGP (mapped Gaussian process) pair style in the Large-scale Atomic/Molecular Massively Parallel Simulator (LAMMPS).[67]

MD simulations were performed using a four-layer slab model of a 21×21 unit cell of Au(111) with a hexagonal Pd_{91} island deposited on the top. The bottommost layer was immobilized to prevent it from acting as a surface. All simulations consist of 1 ns equilibration within the isothermal-isobaric (NPT) ensemble, followed by production within the canonical (NVT) ensemble. Pressure and temperature were enforced on the system with a Nosé-Hoover barostat (1000 δt = 5 ps coupling) and thermostat (100 δt = 0.5 ps coupling), respectively.[63,64,68]

3. Results and discussion

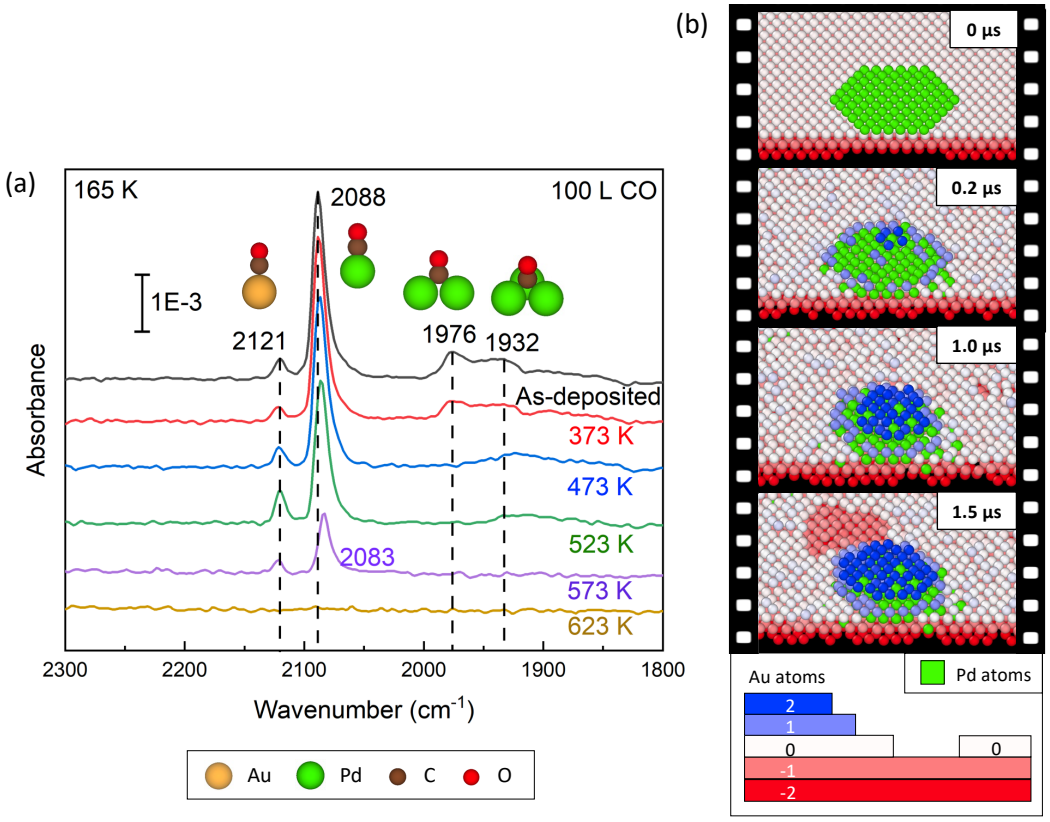

Figure 1. **(a)** IR spectra of low-temperature (165 K) CO adsorption to probe the presence of surface Pd on 0.1 ML Pd/Au(111) at varying stages of annealing. CO exposures were 100 L (1 Langmuir = 1×10^{-6} Torr·s) at 165 K. Upon Pd deposition at room temperature (black), the sample underwent sequential flash annealing in vacuum, starting at 373 K (red) and increasing in temperature until the CO signal was lost at 623 K (gold). As-deposited sample exhibited CO adsorption mainly at Pd atop sites (2088 cm^{-1}) as well as contiguous Pd sites (1976, 1932 cm^{-1}), followed by undercoordinated Au sites (2121 cm^{-1}). Upon annealing, Pd sites decreased in intensity, leaving behind only Pd atop sites by 573 K. **(b)** Machine-learning MD simulation showing the evolution of a monolayer Pd_{91} island on Au(111) at 600 K over 1.5 μs (see video here). A metastable structure was found after the system reached a quasi-equilibrium in ~2 μs: the island became encapsulated by surface Au atoms and partially dissolved into the subsurface, leaving behind isolated Pd monomers and surface vacancy pits.

3.1. Pd dissolves into Au and disperses upon annealing

0.1 ML of Pd was first evaporated onto a clean single-crystal Au(111) at room temperature. Upon Pd deposition, the presence of surface Pd on Au(111) was probed by taking IRRAS spectra after cooling down to 165 K and dosing 100 L of CO. By dosing CO at this temperature, restructuring induced by CO is minimized.[44–46] Due to the preferential binding of CO to Pd over Au, CO vibrational frequencies from IRRAS allow differentiation of the binding sites on Pd ensembles.[47] The spectrum taken for the as-prepared sample (**Fig. 1a**; black) indicates the presence of extended Pd ensembles on the surface. The broad peaks located at lower frequencies correspond to CO adsorption at contiguous Pd sites (~1976 cm^{-1})[69] and multifold sites (~1930 cm^{-1}),[70]

consistent with Pd islands which were shown to form even at a lower Pd coverage of 0.01 ML in a previous STM study.[20] In addition, two sharp peaks were found at 2088 and 2120 cm^{-1}, which are assigned to CO adsorption at Pd atop sites and undercoordinated Au, respectively. The lower one is consistent with our computed value of 2062 cm^{-1} from DFT for CO adsorbed on an isolated Pd atom embedded in the surface layer of Au(111). The Pd atop sites consist of Pd monomers (surrounded by Au) as well as Pd atoms in larger ensembles and islands, both of which were observed previously upon room temperature deposition.[20] On the other hand, the assignment for the highest frequency peak is based on previous studies showing CO adsorption at ~2125 cm^{-1} on Au(111) after Ar^+ sputtering, which creates under-coordinated sites.[71,72] This frequency is higher than that of CO adsorption on Pd atop sites (2102 cm^{-1} on Pd(111)). To verify this, we carried out a control experiment with single-crystal Au(111), for which a peak was observed at 2125 cm^{-1} only after Ar^+ sputtering (**Fig. S1**; blue) and not seen on the flat Au(111) surface (**Fig. S1**; black).

At higher temperatures, Pd has sufficient thermal energy to dissolve into Au and lower the overall surface free energy. Due to the elemental surface energy differential (Pd = 2.05 J/m^2; Au = 1.63 J/m^2),[25] Pd thermodynamically prefers to remain dispersed in the subsurface of Au under reducing conditions.[2] After Pd deposition, the sample underwent sequential flash annealing in vacuum, starting at 373 K and increasing in temperature (**Fig. 1a**; red to gold). At each temperature, the sample was held for a few seconds followed by immediate cooling down to 165 K. The IR spectra were measured at this temperature under UHV after dosing 100 L of CO. The overall CO signal decreased upon annealing and disappeared completely by 623 K, consistent with the dissolution of the Pd islands observed in a previous STM study upon annealing at 450 K.[20] Specifically, the IR bands at 1976 and 1932 cm^{-1} disappeared by 573 K, and the peak at 2088 cm^{-1} was reduced by more than half. Annealing decreased and eventually eliminated above 523 K the contiguous Pd sites (1976 cm^{-1}), which is attributed to the Pd-Au place exchange initiated at the rim of the islands as observed in our simulation discussed below, leaving behind mostly Pd monomers. Concomitantly, the peak assigned to undercoordinated Au sites (2125 cm^{-1}) gained intensity. Similar trends were also observed at higher Pd coverages (see **Sec. 2**, **SI**).

The atomic-level restructuring mechanisms underlying the annealing process were uncovered through machine-learning MD simulations. A mapped Gaussian process model of the Pd/Au potential energy surface was constructed using a recently developed active learning algorithm,[65,66] enabling large-scale and long-timescale simulations at first-principles accuracy (see **Sec. 4**, **SI** for details). Similar to our previous study of Pd/Ag(111),[19] as-deposited Pd island evolved into an immediate metastable structure in 1.5 μs at 600 K (**Fig. 1b**). While this timescale is long for simulations, it is still several orders of magnitude shorter than the experimentally accessible ones. As such, the simulations were carried out at higher temperatures to be able to observe processes seen experimentally in the minute-timescale. Upon becoming encapsulated by surface Au atoms, the island partially dissolved into the subsurface, leaving behind Pd monomers and surface vacancy pits. The restructuring is driven by Pd-Au place exchange events that occur primarily at the edges of the island. Such exchange mechanisms have been shown to be facile at edges and corners, as opposed to flat terraces.[19,37] The resulting Au atoms around the edges and pits are examples of the undercoordinated sites that correspond to the IR peak at 2121 cm^{-1}, which slightly increases in intensity up to 523 K (**Fig. 1a**; black to green). We note that the observed

structure is metastable, and Pd will likely continue to dissolve layer-by-layer over a much longer timescale on the order of minutes, as was observed in a previous kinetic Monte Carlo study of Pd/Cu segregation over 900 s at 500 K.[32]

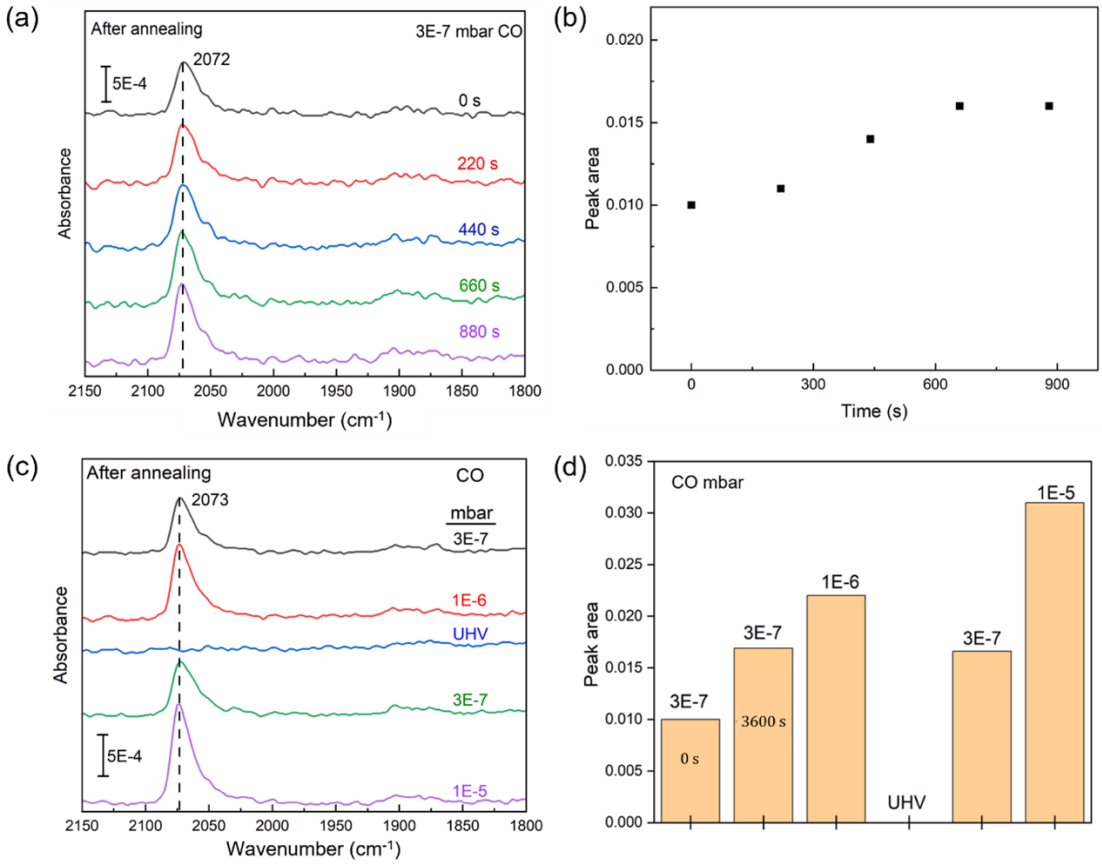

Figure 2. Room-temperature CO adsorption on 0.38 ML Pd deposited on Au(111), after annealing at 473 K for 10 min in vacuum. **(a)** IR spectra measured at 300 K over 1100 s (black to purple) under constant CO pressure of 3×10^{-7} mbar. Only CO adsorption at Pd atop sites (2072 cm^{-1}) was observed. **(b)** The corresponding peak area vs. time; each data point is an average of 1000 scans in 220 s. The first peak area is nonzero because CO saturation occurred much faster than our time resolution of 220 s per spectrum. **(c)** IR spectra measured at 300 K under CO pressure varied sequentially (black to green) after initial equilibration at 3×10^{-7} mbar. **(d)** The corresponding peak area vs. CO pressure; the initial value ($t = 0$ s) at 3×10^{-7} mbar is included as a reference.

3.2. CO-induced segregation of Pd back to the surface

In addition to functioning as a probe molecule, CO can affect the surface restructuring at non-cryogenic temperatures, by providing a thermodynamic driving force that enables Pd to be stabilized on the surface.[20] To determine the feasibility and a representative timescale of such a process, we first investigated the effect of exposure to a constant pressure of CO at room temperature. This was done using a surface with initial coverage of 0.38 ML Pd/Au(111) after it was annealed at 473 K for 10 minutes. The surface was exposed to 3×10^{-7} mbar of CO at 300 K and monitored by sequential IRRAS measurements during a period of 1100 s. CO adsorption occurred only on Pd monomers (**Fig. 2a**; 2072 cm^{-1}), and the corresponding peak area increased over time from 0.0100 to 0.0155 and started plateauing after 880 s (**Fig. 2b**). These observations indicate that CO actively increases the surface concentration of Pd monomers within the time span of ~1000 s at room temperature.

After further equilibrating for 1 hr at 3×10^{-7} mbar (**Fig. 2c**; black), the peak area reached the maximum of 0.0169 from the initial value of 0.010 (**Fig. 2d**). Then, the pressure was varied sequentially at room temperature while measuring consecutive IR spectra until no change in peak area was observed. Overall, higher CO pressure resulted in a larger peak area. E.g., the peak area increased to 0.0220 upon increasing the pressure to 1×10^{-6} mbar (held for ~ 900 s, with the last spectrum taken under this pressure shown in **Fig. 2c**; red). This increase is attributed to not only an increased concentration of surface Pd monomers, but most likely to higher coverage of CO (normalized to the number of surface Pd monomers), given that CO adsorption is a reversible process at room temperature. Upon pumping down the CO from the system, all CO desorbed immediately, as shown by the loss of all IR signals (**Fig. 2c**; blue). Figure S7b shows the calculated coverage of CO (per surface Pd atom, based on DFT results) as a function of pressure from 10^{-8} to 10^{-2} mbar. A significant variation in CO coverage can be seen in the 10^{-8} to 10^{-5} mbar range (from ~0.1 to ~1), establishing that a significant contribution to the change in CO peak area with pressure comes from the change in CO coverage in this pressure range. For comparison, experimental points from Figure 2d are overlayed in Figure S7b.

Upon reintroducing 3×10^{-7} mbar of CO right after the evacuation, CO immediately saturated the same Pd monomer sites (**Fig. 2c**; green; 2073 cm^{-1}). Moreover, the peak area was recovered to 0.0165, close to the pre-evacuation value of 0.0169 (**Fig. 2d**). Given the previously observed long timescale of ~1000 s for the CO-induced migration of additional Pd atoms to the surface (**Fig. 2b**), the rapid saturation of CO suggests that the surface Pd atoms had persisted on the surface or in the near-surface region during the short period of time the sample remained in UHV. Further increasing the pressure to 1×10^{-5} mbar resulted in an increased peak area beyond 0.030 (After holding the pressure for ~ 900 s, **Fig. 2c**; purple), which is likely the result of a combination of additional Pd segregating to the surface, but mainly a CO coverage effect, based on what is shown in Figure S7b and discussed above.

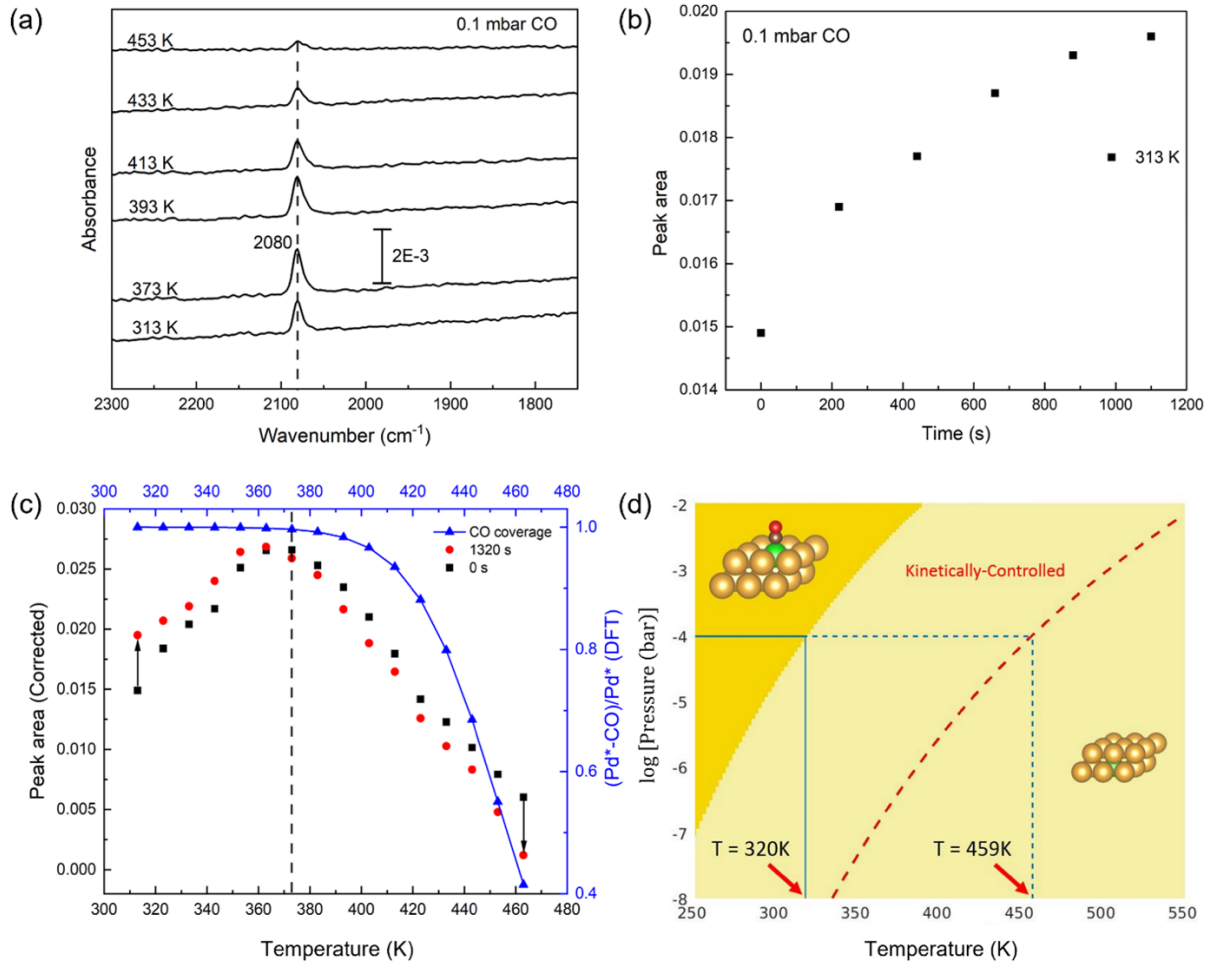

Figure 3. Temperature-programmed IRRAS under constant CO pressure of 0.1 mbar for the annealed 0.1 ML Pd/Au(111). **(a)** The IR spectra exhibited CO adsorption at Pd atop sites (2080 cm^{-1}), with intensity changing as a function of temperature. **(b)** The peak area change over 1320 s, shown for the case of 313 K. Each data point is an average of 1000 scans in 220 s. **(c)** Evolution of the peak area as a function of temperature, increasing from 313 K to 463 K in steps of 10 K and intervals of 1500 s. The black square corresponds to the first spectrum at each temperature, while the red circles correspond to a spectrum taken 1320 s later. The peak area is corrected using the DFT-computed CO adsorption isotherm (blue curve;). Pd segregated to the surface up to 373 K (dashed vertical line), temperature above which dissolution prevailed until complete CO desorption at 473 K. **(d)** Phase diagram computed from *ab initio* thermodynamics for two phases: CO adsorption on Pd monomer (dark yellow) and subsurface Pd with no adsorption (light yellow). At the experimental CO pressure of 1×10^{-4} bar (0.1 mbar), the thermodynamic transition is predicted at 320 K (blue solid line). In the intermediate kinetically controlled regime (bounded by the red dashed line), CO desorption is endergonic and Pd can remain kinetically trapped on the surface. Above 459 K (blue dashed line), CO desorption becomes exergonic, and Pd dissolution is favored.

3.3. Dynamic surface restructuring under CO

Time-resolved temperature-programmed IRRAS experiments were conducted to systematically investigate the dynamics and kinetics of surface segregation as a function of temperature. After annealing at 473 K for 10 min in vacuum, 0.1 ML Pd/Au(111) was exposed to a constant CO pressure of 0.1 mbar, and the temperature was increased from 313 to 473 K in steps of 10 K. At each temperature, six spectra were measured in steps of 220 s to monitor the dynamical change of the surface over the total span of 1320 s. Across all temperatures, CO adsorption occurred only on Pd monomers, and the peak area varied as a function of temperature (**Fig. 3a**; 2080 cm^{-1}). CO exposure did not result in any aggregation of Pd monomers into larger ensembles, as concluded from the absence of the IR band at ~1900 cm^{-1} for contiguous Pd sites.

The surface concentration of Pd monomers exhibited complex behavior as a function of both temperature and time. In terms of temperature, the corresponding peak area increased up to 373 K and started decreasing beyond 373 K (**Fig. 3c**). At each temperature, the rate of change of the peak area diminishes in the span of ~1000 s (e.g. **Fig. 3b** for the case of 313 K), consistent with the timescale observed on the annealed 0.38 ML Pd/Au(111) (**Fig. 2b**). This transient behavior is indicated by the two temperature profiles corresponding to the initial and the final spectra (**Fig. 3c**; black to red, respectively). Specifically, Pd segregated to the surface up to 373 K, above which dissolution prevailed until complete CO desorption at 473 K. In the range of 313-373 K, the thermal mobility is just enough to enable Pd atoms to revisit the surface without dissolving further into the bulk, while allowing CO to adsorb and stabilize the resurfacing Pd atoms. Above 373 K, the peak area decreases with time, indicating Pd dissolution even under the presence of CO. At 473 K, Pd dissolves completely. These measurements shed light on the dynamical evolution of the surface on the timescale of minutes across the relevant temperature range.

A much longer timescale was required for segregation back to the surface once the Pd atoms became dispersed into the deeper subsurface. This is illustrated by the data presented in **Fig. S4,** corresponding to a similar experiment as described above but including a heating and cooling cycle. After complete dissolution at 473 K, surface Pd monomers could be only partially recovered upon cooling under CO, demonstrating a clear hysteresis of the restructuring process. A faster cooling rate was applied by measuring only one spectrum per temperature in the cooling phase, as compared to two in the heating phase (1.8 K/min in the cooling phase compared to 1.1 K/min in the heating phase). Only a fraction of Pd atoms was recovered, ending with a much lower peak area of ~0.005 at 313 K compared to ~0.013 at the start of the experiment (**Fig. S4**). In contrast, no recovery was observed when a slower cooling rate was applied, in steps of 20 K and measuring four spectra per temperature (**Fig. S5a**) (1.2 K/min in the heating phase and 1.2 K/min in the cooling phase). The peak area remained zero throughout the cooling phase, even after waiting for 1 hr at 313 K (**Fig. S5b**). A modest recovery was possible at a higher temperature of 353 K, but only after waiting for a much longer period of 10 hrs (**Fig. S6b**). These observations highlight the sensitivity of the restructuring dynamics to the extent of Pd dissolution into the bulk of Au.

The complete CO desorption at 473 K is attributed to the complete dissolution of Pd, rather than the limited CO adsorption at this temperature. While both could be plausible explanations for what we observed experimentally, we should still be able to see CO adsorption as we cool down

if CO desorption was the cause of the loss of signal. As seen in our room-temperature IRRAS measurements at varying CO pressures (**Fig. 2c-d**), immediate saturation of CO molecules would be expected if Pd remains on the surface, which was not observed during the rapid cooling phases performed after reaching 473 K (**Fig. S5b** and **S6b**). As such, the absence of CO signal here within the established timescale of ~1000 s indicates the absence of surface Pd monomers. We note that the surface concentration of Pd monomers deduced from the CO signal is likely underestimated at higher temperatures where the saturation coverage of CO on Pd becomes lower. To further investigate this issue, we performed a calculation of the CO adsorption isotherm based on DFT energies (**Fig. S7** and **Fig. 3c**; blue) assuming a fixed surface Pd concentration across all temperatures considered. CO coverage on Pd (defined as the fractional occupation (Pd*-CO)/Pd*) decreases with increasing temperature. In particular, less than 90% of available Pd* atoms are occupied by CO molecules at 423 K and above (Indicated by the asterisk symbol in **Fig. S7**). To disentangle the effect of CO desorption from Pd dissolution, our measured peak areas (**Fig. 3c**; black and red) were corrected by dividing them by the computed coverage values (values at corresponding temperatures in **Fig. S7**). By doing so, the complete dissolution of Pd can be established at 463 K and above.

The thermodynamic factors governing the CO-induced segregation of Pd monomers can be understood through the phase diagram computed from DFT calculations (**Fig. 3d**). At the experimental CO pressure of 0.1 mbar, a thermodynamic transition is predicted at 320 K, from CO adsorbed on surface Pd monomers to subsurface Pd monomers with desorbed CO, consistent with the temperature-programmed IRRAS profile. Below 320 K, CO adsorption is capable of stabilizing the Pd monomer on the surface (dark yellow region). At higher temperatures, however, CO adsorption on surface Pd monomers is no longer thermodynamically favored due to the more significant entropic cost arising from the loss of translational and rotational degrees of freedom of the gas-phase CO, combined with the energetic preference of Pd to become dispersed in the subsurface in the absence of CO (light yellow region).

Although thermodynamics dictates the competition between CO adsorption and Pd dissolution, kinetic factors governing interlayer Pd mobility enable CO-bound Pd monomers to persist on the surface above 320 K. Indeed, if Pd is constrained to remain on the surface, complete CO desorption would only occur at 459 K (**Fig. 3d**; blue dashed line). Note that in the adsorption isotherm of fig 3c, the desorption temperature corresponds to a coverage of 0.5. In the experiment, although Pd dissolution initiated above 363 K, the IR peak areas corresponding to CO adsorption on Pd monomers remained nonzero up to 473 K (**Fig. 3c**). Such a scenario is explained through an intermediate kinetically controlled regime, lying between 320 and 459 K at 0.1 mbar in the computed phase diagram (bounded by the red dashed line in **Fig. 3d**). Below 459 K, the migration of CO-bound Pd atom into the subsurface can occur through two different pathways: (a) an endergonic CO desorption, followed by an exergonic Pd dissolution, or (b) an endergonic Pd migration, followed by CO diffusion onto Au and subsequent exergonic desorption. Above 459 K, CO desorption from surface Pd is computed to be exergonic and fast, which would enable complete Pd dissolution, consistent with the observed loss of all CO signals from the IRRAS experiments. The small difference in the computed thermodynamic transition temperature (320 K) and the

experimentally observed value (~360 K) is attributed to the limited accuracy of the calculated free energies.

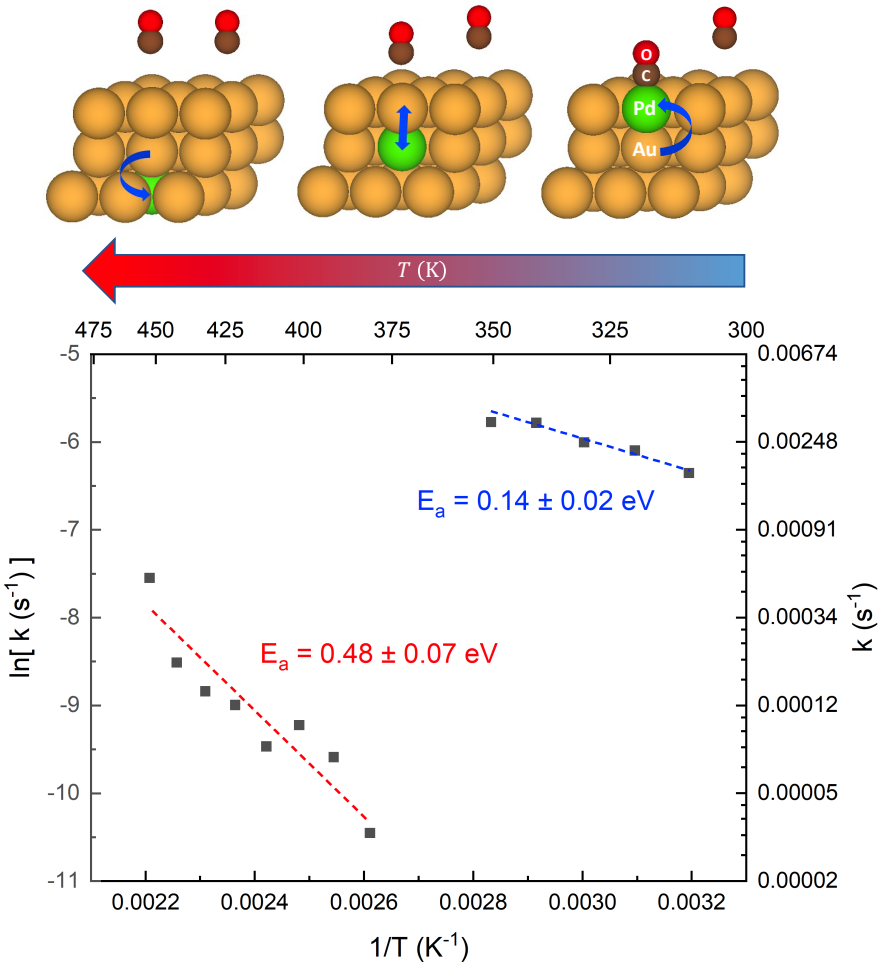

Figure 4. The Arrhenius plot of Pd dissolution observed in the temperature range of 313-453 K under constant CO pressure of 0.1 mbar for the annealed 0.1 ML Pd/Au(111). The apparent activation energies are 0.14 ± 0.02 eV for Pd segregation to the surface below 373 K, and 0.48 ± 0.07 eV for Pd dissolution above 373 K. The pre-exponential factors are $\exp(-1.06 \pm 0.68)$ and $\exp(4.41 \pm 2.09)$ s^{-1}, respectively.

The rate of change of the surface Pd monomer concentration from our temperature-programmed IRRAS data enables the determination of the kinetic parameters associated with the surface restructuring processes. The rate constants were calculated assuming a first-order reaction in which the rate depends linearly on the surface concentration of Pd monomers. The Arrhenius expression of the rate constant is given by

$$k = \nu \exp\left(-\frac{E_\mathrm{a}}{k_\mathrm{B}T}\right),$$

where E_{a} is the apparent activation energy of the process in question, and ν is the pre-exponential factor containing the entropy of activation, S_{a}, based on the Eyring equation:

$$\nu = \frac{k_{\mathrm{B}}T}{h}\exp\left(\frac{S_{\mathrm{a}}}{k_{\mathrm{B}}}\right).$$

The Arrhenius analysis reveals how the segregation of Pd monomers to the surface becomes energetically downhill in the presence of CO (**Fig. 4**). The apparent activation energies were obtained as 0.14 ± 0.02 eV for Pd segregation to the surface below 373 K; and 0.48 ± 0.07 eV for Pd dissolution above 373 K. These barriers can be understood in terms of the Bell-Evans-Polanyi (BEP) principle[73,74] using our DFT-computed segregation energy, defined as the change in energy as a Pd atom (Pd_1) migrates from the subsurface to the surface layer of Au(111), with the concomitant migration of surface-bound CO from Au to the Pd atom:[16]

$$E_{\mathrm{seg}} = E\left[\mathrm{CO}^{\mathrm{Pd_1}}_{(\mathrm{ads})}/\mathrm{Pd}_1^{(\mathrm{surf})}/\mathrm{Au}(111)\right] - E\left[\mathrm{CO}^{\mathrm{Au}}_{(\mathrm{ads})}/\mathrm{Pd}_1^{(\mathrm{sub})}/\mathrm{Au}(111)\right].$$

In the absence of CO, the segregation is endothermic by +0.31 eV, consistent with the higher surface energy of Pd than Au. In contrast, when a CO molecule adsorbs and stabilizes the Pd atom on the surface, the segregation becomes exothermic by –0.46 eV, which means that the reverse process of Pd dissolution is now endothermic by +0.46 eV. Comparing these two reaction energies, the BEP principle suggests that the energetically downhill process of CO-induced segregation ($E_{\mathrm{seg}} = -0.46$ eV) would correspond to a lower energy barrier (measured 0.14 ± 0.02 eV). Conversely, the energetically uphill process of Pd dissolution in the presence of surface-bound CO ($E_{\mathrm{dis}} = +0.46$ eV) would correspond to a higher energy barrier (measured 0.48 ± 0.07 eV).

The pre-exponential factors are also consistent with the nature of the restructuring processes. Specifically, the negative argument of the prefactor $\exp(-1.06 \pm 0.68)$ for reverse segregation indicates a negative change in the configurational entropy, which is expected based on the lower degrees of freedom present on the surface compared to the subsurface. The reverse scenario holds for Pd dissolution where the configurational entropy increases, as seen in the positive argument of the prefactor $\exp(4.41 \pm 2.09)$. The small magnitude of the prefactors is largely attributed to the entropy cost associated with CO adsorption in the presence of adsorbed CO.

4. Conclusions

Bimetallic catalysts are utilized in many industrially important reactions, and catalyst pretreatment with species such as CO has been shown to be a promising strategy of engineering their catalytic performance through dynamic restructuring of the alloy surfaces. However, mechanistic and kinetic studies of such restructuring have remained challenging due to the long timescale and large structural and chemical degrees of freedom that need to be explored. In this

work, we systematically map out the thermodynamics, kinetics, and dynamics of surface restructuring *in situ* by employing time-resolved experimental techniques with surface and chemical sensitivity, as well as first-principles-based modeling and simulations. Our multidisciplinary surface science approach has uncovered previously unknown timescale and kinetic parameters of restructuring in PdAu(111) induced by CO, which translates to an *in situ* control of the active sites in dilute Pd-in-Au nanoparticle catalysts.

Machine-learning molecular dynamics simulations revealed the atomic mechanisms by which as-deposited Pd islands became encapsulated with Au and partially dissolved into the subsurface upon annealing in vacuum. At low Pd coverage, isolated Pd monomers dominated the surface, as observed from infrared reflection absorption spectroscopy (IRRAS) using CO as a low-temperature probe molecule. Subsequent exposure to constant CO pressure at room temperature confirmed the active role of CO in segregating Pd back to the surface. Time-resolved temperature-programmed IRRAS experiments further elucidated the underlying dynamics and kinetics. Under 0.1 mbar CO, Pd monomers segregated to the surface up to 373 K, the temperature above which complete Pd dissolution occurred by 473 K, with apparent activation energies of 0.14 and 0.48 eV, respectively. These restructuring processes occurred over the span of ~1000 s at a given temperature and are consistent with the phase diagram computed from *ab initio* thermodynamics. Such a minute-timescale dynamics highlight the possibility of catalytic processes proceeding on fluxional surfaces[75–78] (provided that the system is below a limiting temperature above which Pd dissolution becomes irreversible), as well as an opportunity to fine-tune the surface composition at moderate temperature and pressure conditions.[16,20] The coupling between surface restructuring dynamics and catalytic transformation of reactants hence appear as an important fundamental aspect of bimetallic catalysts.

Additional information

The Supporting Information is available in the online version of the paper.

CO adsorption on pure Au(111); CO adsorption at higher Pd coverages; additional temperature-programmed IRRAS data; details of machine-learning MD simulation

Acknowledgments

This work was supported by the Integrated Mesoscale Architecture for Sustainable Catalysis (IMASC), an Energy Frontier Research Center (EFRC) funded by the US Department of Energy, Office of Science, Office of Basic Energy Sciences under Award No. DE-SC0012573. Z.D. was supported by ACS PRF grant #61059-ND5. J.S.L. used the Odyssey cluster, FAS Division of Science, Research Computing Group at Harvard University. H.T.N. used the HOFFMAN2 cluster at the UCLA Institute for Digital Research and Education (IDRE). J.S.L. and H.T.N. used the National Energy Research Scientific Computing Center (NERSC), a Department of Energy Office of Science User Facility supported under Contract No. DE-AC02-05CH11231, through allocation

m3275. Experimental work was carried out at the Center for Functional Nanomaterials, Brookhaven National Laboratory, which is supported by the US Department of Energy, Office of Science, Office of Basic Energy Sciences under Contract No. DE-SC0012704. We acknowledge enlightening discussions with all members of the IMASC EFRC.

Competing financial interests

The authors declare no competing financial interests.

References

(1) Luneau, M.; Shirman, T.; Foucher, A. C.; Duanmu, K.; Verbart, D. M. A.; Sautet, P.; Stach, E.; Aizenberg, J.; Madix, R. J.; Friend, C. M. Achieving High Selectivity for Alkyne Hydrogenation at High Conversions with Compositionally Optimized PdAu Nanoparticle Catalysts in Raspberry Colloid Templated SiO2. *ACS Catal.* **2020**, *10* (1), 441–450.

(2) Luneau, M.; Guan, E.; Chen, W.; Foucher, A. C.; Marcella, N.; Shirman, T.; Verbart, D. M. A.; Aizenberg, J.; Aizenberg, M.; Stach, E. A.; Madix, R. J.; Frenkel, A. I.; Friend, C. M. Enhancing Catalytic Performance of Dilute Metal Alloy Nanomaterials. *Commun. Chem.* **2020**, *3* (1), 46. https://doi.org/10.1038/s42004-020-0293-2.

(3) Ni, M.; Leung, D. Y. C.; Leung, M. K. H. A Review on Reforming Bio-Ethanol for Hydrogen Production. *Int. J. Hydrog. Energy* **2007**, *32* (15), 3238–3247. https://doi.org/10.1016/j.ijhydene.2007.04.038.

(4) Wang, C.; Ouyang, M.; Li, M.; Lee, S.; Flytzani-Stephanopoulos, M. Low-Coordinated Pd Catalysts Supported on Zn1Zr1Ox Composite Oxides for Selective Methanol Steam Reforming. *Appl. Catal. A* **2019**, *580*, 81–92. https://doi.org/10.1016/j.apcata.2019.05.006.

(5) Pérez-Temprano, M. H.; Casares, J. A.; Espinet, P. Bimetallic Catalysis Using Transition and Group 11 Metals: An Emerging Tool for C-C Coupling and Other Reactions. *Chem. Eur. J.* **2012**, *18* (7), 1864–1884. https://doi.org/10.1002/chem.201102888.

(6) Luneau, M.; Shirman, T.; Filie, A.; Timoshenko, J.; Chen, W.; Trimpalis, A.; Flytzani-Stephanopoulos, M.; Kaxiras, E.; Frenkel, A. I.; Aizenberg, J.; Friend, C. M.; Madix, R. J. Dilute Pd/Au Alloy Nanoparticles Embedded in Colloid-Templated Porous SiO2: Stable Au-Based Oxidation Catalysts. *Chem. Mater.* **2019**, *31* (15), 5759–5768. https://doi.org/10.1021/acs.chemmater.9b01779.

(7) Luneau, M.; Lim, J. S.; Patel, D. A.; Sykes, E. C. H.; Friend, C. M.; Sautet, P. Guidelines to Achieving High Selectivity for the Hydrogenation of α,β-Unsaturated Aldehydes with Bimetallic and Dilute Alloy Catalysts: A Review. *Chem. Rev.* **2020**, *120* (23), 12834–12872. https://doi.org/10.1021/acs.chemrev.0c00582.

(8) Landon, P.; Collier, P. J.; Carley, A. F.; Chadwick, D.; Papworth, A. J.; Burrows, A.; Kiely, C. J.; Hutchings, G. J. Direct Synthesis of Hydrogen Peroxide from H2 and O2 Using Pd and Au Catalysts. *Phys. Chem. Chem. Phys.* **2003**, *5* (9), 1917–1923. https://doi.org/10.1039/b211338b.

(9) Landon, P.; Collier, P. J.; Papworth, A. J.; Kiely, C. J.; Hutchings, G. J. Direct Formation of Hydrogen Peroxide from H2/O2 Using a Gold Catalyst. *Chem. Commun.* **2002**, No. 18,

2058–2059.
(10) Baddeley, C. J.; Ormerod, R. M.; Stephenson, A. W.; Lambert, R. M. Surface Structure and Reactivity in the Cyclization of Acetylene to Benzene with Pd Overlayers and Pd/Au Surface Alloys on Au{111}. *J. Phys. Chem.* **1995**, *99* (14), 5146–5151. https://doi.org/10.1021/j100014a039.
(11) He, Q.; Chen, W.; Mukerjee, S.; Chen, S.; Laufek, F. Carbon-Supported PdM (M = Au and Sn) Nanocatalysts for the Electrooxidation of Ethanol in High PH Media. *J. Power Sources* **2009**, *187* (2), 298–304. https://doi.org/10.1016/j.jpowsour.2008.11.065.
(12) Ksar, F.; Ramos, L.; Keita, B.; Nadjo, L.; Beaunier, P.; Remita, H. Bimetallic Palladium-Gold Nanostructures: Application in Ethanol Oxidation. *Chem. Mater.* **2009**, *21* (15), 3677–3683. https://doi.org/10.1021/cm901364w.
(13) Liu, J.; Uhlman, M. B.; Montemore, M. M.; Trimpalis, A.; Giannakakis, G.; Shan, J.; Cao, S.; Hannagan, R. T.; Sykes, E. C. H.; Flytzani-Stephanopoulos, M. Integrated Catalysis-Surface Science-Theory Approach to Understand Selectivity in the Hydrogenation of 1-Hexyne to 1-Hexene on PdAu Single-Atom Alloy Catalysts. *ACS Catal.* **2019**, *9* (9), 8757–8765. https://doi.org/10.1021/acscatal.9b00491.
(14) Neurock, M. Perspectives on the First Principles Elucidation and the Design of Active Sites. *J. Catal.* **2003**, *216* (1–2), 73–88. https://doi.org/10.1016/S0021-9517(02)00115-X.
(15) van der Hoeven, J. E. S.; Ngan, H. T.; Taylor, A.; Eagan, N. M.; Aizenberg, J.; Sautet, P.; Madix, R. J.; Friend, C. M. Entropic Control of HD Exchange Rates over Dilute Pd-in-Au Alloy Nanoparticle Catalysts. *ACS Catal.* **2021**, *11* (12), 6971–6981. https://doi.org/10.1021/acscatal.1c01400.
(16) Ouyang, M.; Papanikolaou, K. G.; Boubnov, A.; Hoffman, A. S.; Giannakakis, G.; Bare, S. R.; Stamatakis, M.; Flytzani-Stephanopoulos, M.; Sykes, E. C. H. Directing Reaction Pathways via in Situ Control of Active Site Geometries in PdAu Single-Atom Alloy Catalysts. *Nat. Commun.* **2021**, *12* (1), 1549. https://doi.org/10.1038/s41467-021-21555-z.
(17) Baber, A. E.; Tierney, H. L.; Lawton, T. J.; Sykes, E. C. H. An Atomic-Scale View of Palladium Alloys and Their Ability to Dissociate Molecular Hydrogen. *ChemCatChem* **2011**, *3* (3), 607–614. https://doi.org/10.1002/cctc.201000309.
(18) Personick, M. L.; Montemore, M. M.; Kaxiras, E.; Madix, R. J.; Biener, J.; Friend, C. M. Catalyst Design for Enhanced Sustainability through Fundamental Surface Chemistry. *Philos. Trans. R. Soc., A* **2016**, *374* (2061), 20150077. https://doi.org/10.1098/rsta.2015.0077.
(19) Lim, J. S.; Vandermause, J.; van Spronsen, M. A.; Musaelian, A.; Xie, Y.; Sun, L.; O'Connor, C. R.; Egle, T.; Molinari, N.; Florian, J.; Duanmu, K.; Madix, R. J.; Sautet, P.; Friend, C. M.; Kozinsky, B. Evolution of Metastable Structures at Bimetallic Surfaces from Microscopy and Machine-Learning Molecular Dynamics. *J. Am. Chem. Soc.* **2020**, *142* (37), 15907–15916.
(20) van Spronsen, M. A.; Daunmu, K.; O'Connor, C. R.; Egle, T.; Kersell, H.; Oliver-Meseguer, J.; Salmeron, M. B.; Madix, R. J.; Sautet, P.; Friend, C. M. Dynamics of Surface Alloys: Rearrangement of Pd/Ag(111) Induced by CO and O2. *J. Phys. Chem. C* **2019**, *123*, 8312–8323. https://doi.org/10.1021/acs.jpcc.8b08849.
(21) Tao, F.; Grass, M. E.; Zhang, Y.; Butcher, D. R.; Renzas, J. R.; Liu, Z.; Chung, J. Y.; Mun, B. S.; Salmeron, M.; Somorjai, G. A. Reaction-Driven Restructuring of Rh-Pd and Pt-Pd Core-Shell Nanoparticles. *Science (80-.).* **2008**, *322* (5903), 932–934. https://doi.org/10.1126/science.1164170.

(22) Tao, F.; Zhang, S.; Luan, N.; Zhang, X. Action of Bimetallic Nanocatalysts under Reaction Conditions and during Catalysis: Evolution of Chemistry from High Vacuum Conditions to Reaction Conditions. *Chem. Soc. Rev.* **2012**, *41* (24), 7980–7993. https://doi.org/10.1039/c2cs35185d.
(23) Zafeiratos, S.; Piccinin, S.; Teschner, D. Alloys in Catalysis: Phase Separation and Surface Segregation Phenomena in Response to the Reactive Environment. *Catal. Sci. Technol.* **2012**, *2* (9), 1787–1801. https://doi.org/10.1039/c2cy00487a.
(24) Vignola, E.; Steinmann, S. N.; Le Mapihan, K.; Vandegehuchte, B. D.; Curulla, D.; Sautet, P. Acetylene Adsorption on Pd-Ag Alloys: Evidence for Limited Island Formation and Strong Reverse Segregation from Monte Carlo Simulations. *J. Phys. Chem. C* **2018**, *122* (27), 15456–15463. https://doi.org/10.1021/acs.jpcc.8b04108.
(25) Tyson, W. R.; Miller, W. A. Surface Free Energies of Solid Metals: Estimation from Liquid Surface Tension Measurements. *Surf. Sci.* **1977**, *62* (1), 267–276. https://doi.org/10.1016/0039-6028(77)90442-3.
(26) Piednoir, A.; Languille, M. A.; Piccolo, L.; Valcarcel, A.; Aires, F. J. C. S.; Bertolini, J. C. Pd(111) versus Pd-Au(111) in Carbon Monoxide Oxidation under Elevated Pressures. *Catal. Letters* **2007**, *114* (1–2), 110–114. https://doi.org/10.1007/s10562-007-9047-3.
(27) Li, Z.; Gao, F.; Furlong, O.; Tysoe, W. T. Adsorption of Carbon Monoxide Au/Pd(100) Alloys in Ultrahigh Vacuum: Identification of Adsorption Sites. *Surf. Sci.* **2010**, *604* (2), 136–143. https://doi.org/10.1016/j.susc.2009.10.031.
(28) Doherty, R. P.; Krafft, J.-M.; Méthivier, C.; Casale, S.; Remita, H.; Louis, C.; Thomas, C. On the Promoting Effect of Au on CO Oxidation Kinetics of Au–Pt Bimetallic Nanoparticles Supported on SiO2: An Electronic Effect? *J. Catal.* **2012**, *287*, 102–113. https://doi.org/https://doi.org/10.1016/j.jcat.2011.12.011.
(29) Creemers, C.; Deurinck, P. Platinum Segregation to the (111) Surface of Ordered Pt80Fe20: LEIS Results and Model Simulations. *Surf. Inter* **1997**, *25* (3), 177–190. https://doi.org/10.1002/(SICI)1096-9918(199703)25:3<177::AID-SIA219>3.0.CO;2-T.
(30) Hirschl, R.; Delbecq, F.; Sautet, P.; Hafner, J. Adsorption of Unsaturated Aldehydes on the (111) Surface of a Pt-Fe Alloy Catalyst from First Principles. *J. Catal.* **2003**, *217* (2), 354–366. https://doi.org/10.1016/S0021-9517(03)00057-5.
(31) Kim, H. Y.; Henkelman, G. CO Adsorption-Driven Surface Segregation of Pd on Au/Pd Bimetallic Surfaces: Role of Defects and Effect on CO Oxidation. *ACS Catal.* **2013**, *3* (11), 2541–2546. https://doi.org/10.1021/cs4006259.
(32) Cheng, F.; He, X.; Chen, Z.-X.; Huang, Y.-G. Kinetic Monte Carlo Simulation of Surface Segregation in Pd-Cu Alloys. *J. Alloy. Compd.* **2015**, *648*, 1090–1096. https://doi.org/10.1016/j.jallcom.2015.05.286.
(33) An, H.; Ha, H.; Yoo, M.; Kim, H. Y. Understanding the Atomic-Level Process of CO-Adsorption-Driven Surface Segregation of Pd in (AuPd)147 Bimetallic Nanoparticles. *Nanoscale* **2017**, *9* (33), 12077–12086. https://doi.org/10.1039/c7nr04435f.
(34) Xu, C.-Q.; Lee, M.-S.; Wang, Y.-G.; Cantu, D. C.; Li, J.; Glezakou, V.-A.; Rousseau, R. Structural Rearrangement of Au–Pd Nanoparticles under Reaction Conditions: An Ab Initio Molecular Dynamics Study. *ACS Nano* **2017**, *11* (2), 1649–1658. https://doi.org/10.1021/acsnano.6b07409.
(35) Wexler, R. B.; Qiu, T.; Rappe, A. M. Automatic Prediction of Surface Phase Diagrams Using Ab Lnitio Grand Canonical Monte Carlo. *J. Phys. Chem. C* **2019**, *123* (4), 2321–2328. https://doi.org/10.1021/acs.jpcc.8b11093.

(36) Yang, Y.; Shen, X.; Han, Y.-F. Diffusion Mechanisms of Metal Atoms in Pd Au Bimetallic Catalyst under CO Atmosphere Based on Ab Initio Molecular Dynamics. *Appl. Surf. Sci.* **2019**, *483*, 991–1005. https://doi.org/10.1016/j.apsusc.2019.04.036.
(37) Lim, J. S.; Molinari, N.; Duanmu, K.; Sautet, P.; Kozinsky, B. Automated Detection and Characterization of Surface Restructuring Events in Bimetallic Catalysts. *J. Phys. Chem. C* **2019**, *123* (26), 16332–16344. https://doi.org/10.1021/acs.jpcc.9b04863.
(38) Mamatkulov, M.; Yudanov, I. V; Bukhtiyarov, A. V; Prosvirin, I. P.; Bukhtiyarov, V. I.; Neyman, K. M. Pd Segregation on the Surface of Bimetallic PdAu Nanoparticles Induced by Low Coverage of Adsorbed CO. *J. Phys. Chem. C* **2019**, *123* (13), 8037–8046. https://doi.org/10.1021/acs.jpcc.8b07402.
(39) García-Mota, M.; López, N. Temperature and Pressure Effects in CO Titration of Ensembles in PdAu(111) Alloys Using First Principles. *Phys. Rev. B* **2010**, *82* (7), 075411. https://doi.org/10.1103/PhysRevB.82.075411.
(40) Ham, H. C.; Stephens, J. A.; Hwang, G. S.; Han, J.; Nam, S. W.; Lim, T. H. Role of Small Pd Ensembles in Boosting CO Oxidation in AuPd Alloys. *J. Phys. Chem. Lett.* **2012**, *3* (5), 566–570. https://doi.org/10.1021/jz201585q.
(41) Meng, J.; Zhu, B.; Gao, Y. Surface Composition Evolution of Bimetallic Alloys under Reaction Conditions. *J. Phys. Chem. C* **2019**, *123* (46), 28241–28247. https://doi.org/10.1021/acs.jpcc.9b08398.
(42) Lu, Z.; Yadav, S.; Singh, C. V. Predicting Aggregation Energy for Single Atom Bimetallic Catalysts on Clean and O* Adsorbed Surfaces through Machine Learning Models. *Catal. Sci. Technol.* **2020**, *10* (1), 86–98. https://doi.org/10.1039/c9cy02070e.
(43) Darby, M. T.; Sykes, E. C. H.; Michaelides, A.; Stamatakis, M. Carbon Monoxide Poisoning Resistance and Structural Stability of Single Atom Alloys. *Top. Catal.* **2018**, *61* (5–6), 428–438. https://doi.org/10.1007/s11244-017-0882-1.
(44) Tenney, S. A.; Ratliff, J. S.; Roberts, C. C.; He, W.; Ammal, S. C.; Heyden, A.; Chen, D. A. Adsorbate-Induced Changes in the Surface Composition of Bimetallic Clusters: Pt-Au on TiO2(110). *J. Phys. Chem. C* **2010**, *114* (49), 21652–21663. https://doi.org/10.1021/jp108939h.
(45) Tenney, S. A.; He, W.; Roberts, C. C.; Ratliff, J. S.; Shah, S. I.; Shafai, G. S.; Turkowski, V.; Rahman, T. S.; Chen, D. A. CO-Induced Diffusion of Ni Atoms to the Surface of Ni-Au Clusters on TiO2(110). *J. Phys. Chem. C* **2011**, *115* (22), 11112–11123. https://doi.org/10.1021/jp2014258.
(46) Galhenage, R. P.; Ammal, S. C.; Yan, H.; Duke, A. S.; Tenney, S. A.; Heyden, A.; Chen, D. A. Nucleation, Growth, and Adsorbate-Induced Changes in Composition for Co-Au Bimetallic Clusters on TiO2. *J. Phys. Chem. C* **2012**, *116* (46), 24616–24629. https://doi.org/10.1021/jp307888p.
(47) Ma, Y.; Diemant, T.; Bansmann, J.; Behm, R. J. The Interaction of CO with PdAg/Pd(111) Surface Alloys-A Case Study of Ensemble Effects on a Bimetallic Surface. *Phys. Chem. Chem. Phys.* **2011**, *13* (22), 10741–10754. https://doi.org/10.1039/c1cp00009h.
(48) Wang, M.; Zhou, C.; Akter, N.; Tysoe, W. T.; Boscoboinik, J. A.; Lu, D. Mechanism of the Accelerated Water Formation Reaction under Interfacial Confinement. *ACS Catal.* **2020**, *10* (11), 6119–6128. https://doi.org/10.1021/acscatal.9b05289.
(49) Kaichev, V. V; Prosvirin, I. P.; Bukhtiyarov, V. I.; Unterhalt, H.; Rupprechter, G.; Freund, H. J. High-Pressure Studies of CO Adsorption on Pd(111) by X-Ray Photoelectron

Spectroscopy and Sum-Frequency Generation. *J. Phys. Chem. B* **2003**, *107* (15), 3522–3527. https://doi.org/10.1021/jp021992t.
(50) Hohenberg, P.; Kohn, W. Inhomogeneous Electron Gas. *Phys. Rev. B* **1964**, *136* (3B), B864. https://doi.org/10.1103/PhysRev.136.B864.
(51) Kresse, G.; Furthmüller, J. Efficient Iterative Schemes for Ab Initio Total-Energy Calculations Using a Plane-Wave Basis Set. *Phys. Rev. B* **1996**, *54* (16), 11169–11186. https://doi.org/10.1103/PhysRevB.54.11169.
(52) Kresse, G.; Hafner, J. Ab Initio Molecular Dynamics for Liquid Metals. *Phys. Rev. B* **1993**, *193*, 222–229. https://doi.org/10.1016/0022-3093(95)00355-X.
(53) Monkhorst, H. J.; Pack, J. D. Special Points for Brillouin-Zone Integrations. *Phys. Rev. B* **1976**, *13* (12), 5188–5192. https://doi.org/10.1103/PhysRevB.13.5188.
(54) Perdew, J. P.; Burke, K.; Ernzerhof, M. Generalized Gradient Approximation Made Simple. *Phys. Rev. Lett.* **1996**, *77* (18), 3865–3868. https://doi.org/10.1103/PhysRevLett.77.3865.
(55) Steinmann, S. N.; Corminboeuf, C. Comprehensive Bench Marking of a Density-Dependent Dispersion Correction. *J. Chem. Theory Comput.* **2011**, *7* (11), 3567–3577. https://doi.org/10.1021/ct200602x.
(56) Steinmann, S. N.; Corminboeuf, C. A Generalized-Gradient Approximation Exchange Hole Model for Dispersion Coefficients. *J. Chem. Phys.* **2011**, *134* (4), 044117. https://doi.org/10.1063/1.3545985.
(57) Gautier, S.; Steinmann, S. N.; Michel, C.; Fleurat-Lessard, P.; Sautet, P. Molecular Adsorption at Pt(111). How Accurate Are DFT Functionals? *Phys. Chem. Chem. Phys.* **2015**, *17* (43), 28921–28930. https://doi.org/10.1039/c5cp04534g.
(58) Feibelman, P. J.; Hammer, B.; Norskov, J. K.; Wagner, F.; Scheffler, M.; Stumpf, R.; Watwe, R.; Dumesic, J. The CO/Pt(111) Puzzle. *J. Phys. Chem. B* **2001**, *105* (18), 4018–4025. https://doi.org/10.1021/jp002302t.
(59) Mason, S. E.; Grinberg, I.; Rappe, A. M. First-Principles Extrapolation Method for Accurate CO Adsorption Energies on Metal Surfaces. *Phys. Rev. B* **2004**, *69* (16), 161401. https://doi.org/10.1103/PhysRevB.69.161401.
(60) Talbi, D.; Chandler, G. S. Extensive Ab Initio Study of the C2O2, C2S2, and C2OS Systems: Stabilities and Singlet-Triplet Energy Gaps. *J. Phys. Chem. A* **2000**, *104* (24), 5872–5881. https://doi.org/10.1021/jp000732d.
(61) Csonka, G. I.; Perdew, J. P.; Ruzsinszky, A.; Philipsen, P. H. T.; Lebègue, S.; Paier, J.; Vydrov, O. A.; Ángyán, J. G. Assessing the Performance of Recent Density Functionals for Bulk Solids. *Phys. Rev. B* **2009**, *79* (15), 1–14. https://doi.org/10.1103/PhysRevB.79.155107.
(62) Kittel, C. *Introduction to Solid State Physics*, 8th ed.; Wiley, 2004.
(63) Nosé, S. A Unified Formulation of the Constant Temperature Molecular-Dynamics Methods. *J. Chem. Phys.* **1984**, *81* (1), 511–519. https://doi.org/10.1063/1.447334.
(64) Hoover, W. G. Canonical Dynamics - Equilibrium Phase-Space Distributions. *Phys. Rev. A* **1985**, *31* (3), 1695–1697. https://doi.org/10.1103/PhysRevA.31.1695.
(65) Vandermause, J.; Torrisi, S. B.; Batzner, S.; Xie, Y.; Sun, L.; Kolpak, A. M.; Kozinsky, B. On-the-Fly Active Learning of Interpretable Bayesian Force Fields for Atomistic Rare Events. *NPJ Comput. Mater.* **2020**, *6* (11), 20. https://doi.org/10.1038/s41524-020-0283-z.
(66) Xie, Y.; Vandermause, J.; Sun, L.; Cepellotti, A.; Kozinsky, B. Bayesian Force Fields from Active Learning for Simulation of Inter-Dimensional Transformation of Stanene.

NPJ Comput. Mater. **2021**, *7* (1), 40. https://doi.org/10.1038/s41524-021-00510-y.
(67) Plimpton, S. Fast Parallel Algorithms for Short-Range Molecular Dynamics. *J. Comput. Phys.* **1995**, *117* (1), 1–19. https://doi.org/10.1006/jcph.1995.1039.
(68) Hoover, W. G. Constant-Pressure Equations of Motion. *Phys. Rev. A* **1986**, *34* (3), 2499–2500. https://doi.org/10.1103/PhysRevA.34.2499.
(69) Wei, T.; Wang, J.; Goodman, D. W. Characterization and Chemical Properties of Pd-Au Alloy Surfaces. *J. Phys. Chem. C* **2007**, *111* (25), 8781–8788. https://doi.org/10.1021/jp067177l.
(70) Szanyi, J.; Kuhn, W. K.; Goodman, D. W. CO Adsorption on Pd(111) and Pd(100): Low and High Pressure Correlations. *J. Vac. Sci. Technol. A Vacuum, Surfaces, Film.* **1993**, *11* (4), 1969–1974. https://doi.org/10.1116/1.578532.
(71) Yim, W.-L.; Nowitzki, T.; Necke, M.; Schnars, H.; Nickut, P.; Biener, J.; Biener, M. M.; Zielasek, V.; Al-Shamery, K.; Klüner, T.; Bäumer, M. Universal Phenomena of CO Adsorption on Gold Surfaces with Low-Coordinated Sites. *J. Phys. Chem. C* **2007**, *111* (1), 445–451. https://doi.org/10.1021/jp0665729.
(72) Hrbek, J.; Hoffmann, F. M.; Park, J. B.; Liu, P.; Stacchiola, D.; Hoo, Y. S.; Ma, S.; Nambu, A.; Rodriguez, J. A.; White, M. G. Adsorbate-Driven Morphological Changes of a Gold Surface at Low Temperatures. *J. Am. Chem. Soc.* **2008**, *130* (51), 17272–17273. https://doi.org/10.1021/ja8081268.
(73) Bell, R. P.; Hinshelwood, C. N. The Theory of Reactions Involving Proton Transfers. *Proc. R. Soc. London. Ser. A - Math. Phys. Sci.* **1936**, *154* (882), 414–429. https://doi.org/10.1098/rspa.1936.0060.
(74) Evans, M. G.; Polanyi, M. Further Considerations on the Thermodynamics of Chemical Equilibria and Reaction Rates. *Trans. Faraday Soc.* **1936**, *32* (0), 1333–1360. https://doi.org/10.1039/TF9363201333.
(75) Zhao, W.; Chizallet, C.; Sautet, P.; Raybaud, P. Dehydrogenation Mechanisms of Methyl-Cyclohexane on Gamma-Al2O3 Supported Pt-13: Impact of Cluster Ductility. *J. Catal.* **2019**, *370*, 118–129. https://doi.org/10.1016/j.jcat.2018.12.004.
(76) Sun, G.; Alexandrova, A. N.; Sautet, P. Structural Rearrangements of Subnanometer Cu Oxide Clusters Govern Catalytic Oxidation. *ACS Catal.* **2020**, *10* (9), 5309–5317. https://doi.org/10.1021/acscatal.0c00824.
(77) Guo, H.; Sautet, P.; Alexandrova, A. N. Reagent-Triggered Isomerization of Fluxional Cluster Catalyst via Dynamic Coupling. *J. Phys. Chem. Lett.* **2020**, *11* (8), 3089–3094. https://doi.org/10.1021/acs.jpclett.0c00548.
(78) Sun, G.; Fuller III, J. T.; Alexandrova, A. N.; Sautet, P. Global Activity Search Uncovers Reaction Induced Concomitant Catalyst Restructuring for Alkane Dissociation on Model Pt Catalysts. *ACS Catal.* **2021**, *11* (3), 1877–1885. https://doi.org/10.1021/acscatal.0c05421.